

Observed and modelled stability of overflow across the Greenland–Scotland ridge

Steffen M. Olsen¹, Bogi Hansen², Detlef Quadfasel³ & Svein Østerhus⁴

Across the Greenland–Scotland ridge there is a continuous flow of cold dense water, termed ‘overflow’, from the Nordic seas to the Atlantic Ocean¹. This is a main contributor to the production of North Atlantic Deep Water² that feeds the lower limb of the Atlantic meridional overturning circulation, which has been predicted to weaken as a consequence of climate change^{3,4}. The two main overflow branches pass the Denmark Strait and the Faroe Bank channel. Here we combine results from direct current measurements in the Faroe Bank channel⁵ for 1995–2005 with an ensemble hindcast experiment⁶ for 1948–2005 using an ocean general circulation model. For the overlapping period we find a convincing agreement between model simulations and observations on monthly to interannual timescales. Both observations and model data show no significant trend in volume transport. In addition, for the whole 1948–2005 period, the model indicates no persistent trend in the Faroe Bank channel overflow or in the total overflow transport, in agreement with the few available historical observations. Deepening isopycnals in the Norwegian Sea have tended to decrease the pressure difference across the Greenland–Scotland ridge⁷, but this has been compensated for by the effect of changes in sea level. In contrast with earlier studies^{7,8}, we therefore conclude that the Faroe Bank channel overflow, and also the total overflow, did not decrease consistently from 1950 to 2005, although the model does show a weakening total Atlantic meridional overturning circulation as a result of changes south of the Greenland–Scotland ridge.

According to observations, the total volume transport of overflow water across the Greenland–Scotland ridge (GSR)¹ is about 6 Sv (1 Sv (sverdrup) = $10^6 \text{ m}^3 \text{ s}^{-1}$) (Fig. 1a). Half of this passes through the Denmark Strait; the other half crosses the ridge east of Iceland through several passages, mainly through the Faroe Bank channel (FBC). At the sill of the FBC, the overflow current is only about 10 km wide (Fig. 1b), which is comparable to the baroclinic Rossby radius. This permits accurate monitoring of volume transport with limited instrumentation⁵. Since 1995 an acoustic Doppler current profiler has been continuously moored in the centre of the channel over the sill (site B; Fig. 1b). Combined with an extensive suite of short-term experiments and hydrographic monitoring, this has permitted the generation of a time series of the overflow volume transport of high accuracy⁵, with a mean transport of 2.1 Sv (Fig. 2a). In addition to the FBC overflow, the eastern overflow includes a total of 1.3 Sv of overflow across the Wyville Thomson ridge (0.3 Sv (ref. 9)) and the Iceland–Faroe ridge (1 Sv (refs 10–12)). These shallow overflows are intermittent and are dominated by synoptic-scale processes rather than the more stable forcing maintaining the overflows in the Denmark Strait and the FBC. No long-term direct transport observations exist; we therefore have no information on flow variability on timescales above seasonal.

A second independent estimate of the overflow transport stems from an ensemble hindcast simulation⁶ for the period 1948–2005 with the use of a global coupled ocean–sea–ice model¹³ forced by atmospheric reanalysis data and observed Arctic river discharges⁶

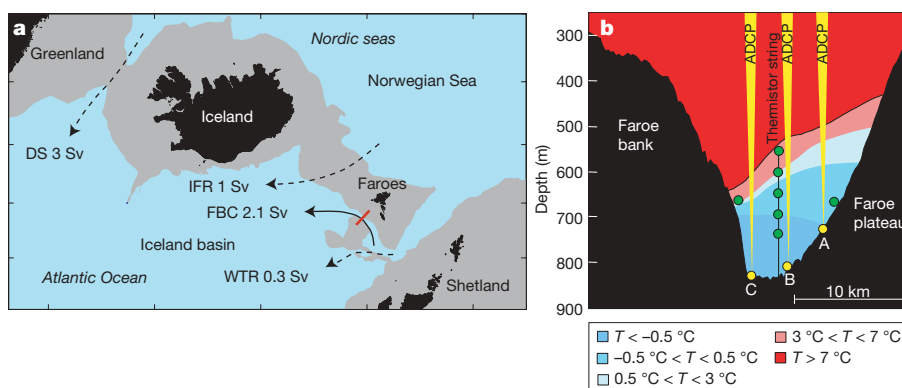


Figure 1 | The GSR overflow branches. **a**, Map of the GSR, with overflow branches indicated by arrows. Numbers give the typical volume transports of each branch^{5,9–12,20}. The solid arrow shows the FBC overflow; dashed arrows indicate the Wyville Thomson ridge (WTR), the Iceland–Faroe ridge (IFR) and Denmark Strait (DS) overflows. The grey area is shallower than 750 m. The red line indicates the monitoring section in the FBC at the sill. **b**, On this

section, instruments have been moored for periods of up to 10 years. Yellow circles indicate the positions of moored acoustic Doppler current profilers with sound beams illustrated by yellow cones. Green circles show the locations of moored temperature sensors. Background colours show the typical temperature distribution on the section.

¹Danish Meteorological Institute, Lyngbyvej 100, 2100 Copenhagen, Denmark. ²Farøese Fisheries Laboratory, Box 3051, FO-110 Tórshavn, Farøe Islands. ³Universität Hamburg, Zentrum für Meeres- und Klimaforschung, Bundesstrasse 53, D-20146 Hamburg, Germany. ⁴Bjerknes Centre for Climate Research, University of Bergen, NO-5014 Bergen, Norway.

(see Methods). Individual exchange branches of Atlantic, overflow and polar waters are diagnosed from the simulation by using temperature and salinity characteristics. The ensemble mean climatology of exchanges⁶, including a total overflow across the GSR of 6.0 Sv and a net Atlantic inflow of 8.7 Sv, compares favourably with existing observations^{1,14}. The model does not separate the various overflows east of Iceland, owing to limited grid resolution. It provides a time series of total eastern overflow with an ensemble mean transport of 3.4 Sv for the period 1995–2005. This is consistent with observations of the combined eastern overflow transport (Fig. 1a). Subtracting the mean overflow across the shallow ridges (1.3 Sv) from the total, we generated a time series of computed FBC overflow (Fig. 2a).

The correspondence between this time series of FBC overflow and the observational series for 1995–2005 is remarkable and can be verified independently to arise from identical seasonality and highly correlated monthly and interannual variability (see Methods). On monthly scales, the correlation coefficient calculated by using de-seasoned data is 0.72 ($P < 10^{-7}$), whereas annual mean data

(Fig. 2a) show an even higher correlation of 0.92 ($P < 10^{-4}$). The statistical analysis confirms that this is extremely unlikely to occur by chance. No individual ensemble member fits the observations better than the ensemble mean (Supplementary Fig. 1), in which internal model variability is practically eliminated (Supplementary Fig. 2). Internal variability may have different sources but is not examined in detail (see Methods). Clearly, however, ensemble averaging allows a very accurate representation of the FBC overflow, which is a strongly forced system with relatively small internal variability.

The trends in both series are equal, weak and not significantly different from zero (0.01 ± 0.02 Sv per decade). The highly significant correlations between two independently produced time series verify the accuracy of both series conclusively. This also implies that the FBC overflow has not changed consistently during the 1995–2005 period. Encouraged by the excellent agreement between model and observations, we used the model data back to 1948 to estimate long-term variations in both the FBC and the total overflow transports (Fig. 2b). Here, the estimated trend of the FBC overflow is found to be positive but again barely distinguishable from zero (0.05 ± 0.02 Sv per decade). For the early period, direct estimates of FBC overflow are few and not of the same proven quality as after 1995, but they do agree with the model time series (Fig. 2b).

This result of no detectable long-term trend in the overflow contradicts earlier reported weakening⁷ of the FBC overflow and is hard to reconcile with measurements indicating a marked decrease⁸ in the Atlantic meridional overturning circulation (AMOC) at 25°N, results that have also been questioned by other studies¹⁵. To understand this discrepancy we performed an analysis of the forcing of the overflow. Theoretical arguments^{5,7,16–20} imply that the FBC overflow transport is related to the pressure difference (ΔP) between both sides of the GSR at the depth of the overflow core. This includes a barotropic component (ΔP_{trop}) determined by the sea level and a baroclinic component (ΔP_{clin}) given by the density field ($\Delta P = \Delta P_{\text{trop}} + \Delta P_{\text{clin}}$). The model shows an almost linear relationship between the overflow transport and the total pressure difference (ΔP) (Fig. 3b). Local and remote processes such as convection, mixing and the circulation in the basins north and south of the ridge contribute to determining the pressure difference; however, once given, it specifies the FBC overflow.

According to the model, the baroclinic component has an overall decreasing trend between 1948 and 2005 (Fig. 3a), consistent with earlier reports⁷. In contrast, the barotropic pressure gradient shows an increasing trend of equal magnitude, so the pressure difference at depth does not have a significant trend. This compensating effect of barotropic and baroclinic contributions to the pressure difference is a striking feature of the time series on timescales from a few years to decades (Fig. 3a). Wind stress affects the strength of the open ocean gyres and, through geostrophy, determines the local sea-level topography including the barotropic pressure difference across the GSR²¹. With some time lag, the density field adjusts to compensate partly for barotropic variations (Fig. 3a). A closer analysis of the pressure difference variations in the model (Fig. 4) reveals that most of the variation originates in the Nordic seas. The changes are of basin-wide scale, and the strong tendency of compensation (Fig. 3a) is thus independent of the specific positions chosen to calculate the cross-ridge pressure variations. Since 1948 the model sea level over most of the Nordic seas showed a positive trend (Fig. 4a), although not monotonic (Fig. 3a); however, adjustment of the density field (Fig. 4b) by lowering isopycnal surfaces led to the maintenance of a relatively stable overflow on timescales above a few years. This timescale of adjustment is quantified in a conceptual framework and explains the main features of Fig. 3a (see Methods).

The conclusion of a relatively stable FBC overflow since 1948 is based on the model results and is corroborated by early, direct estimates of the transport (Fig. 2b). In addition, variations in the pressure difference that forces the overflow can be further validated against observations. Open-ocean sea-level gradients derived from

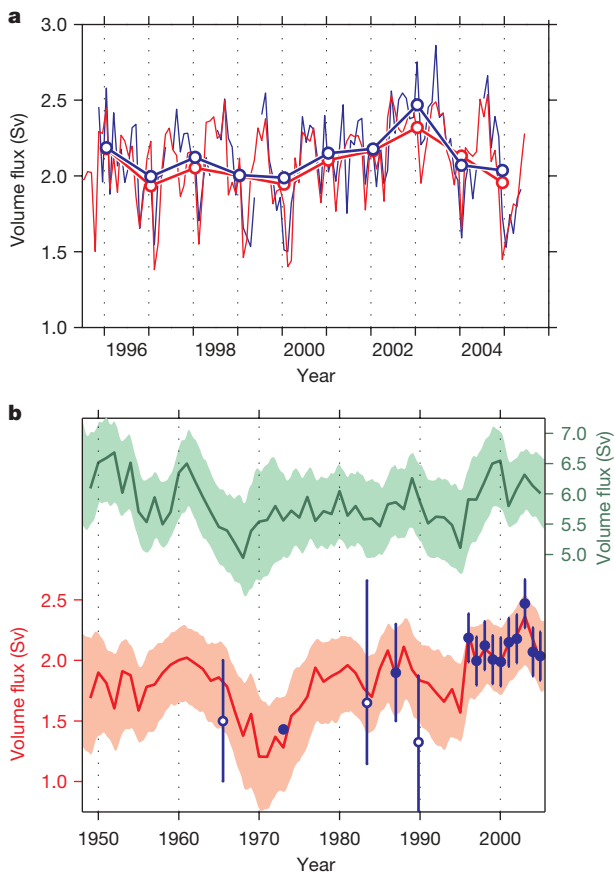


Figure 2 | Observed and computed deep overflow. **a**, Monthly mean observations of the FBC overflow (thin blue lines) and a time series (thin red lines) computed by subtracting 1.3 Sv from the ensemble mean modelled eastern overflow in the instrumental period. Annual mean values (connected circles) are included. Here, data are averaged for months where observations exist (July to May). **b**, Annual FBC overflow transport (red) and total overflow transport across the GSR (green) for 1948–2005, computed on the basis of ensemble means. The ensemble spread between members is represented by coloured shading (2σ). Blue filled circles show all published, long-term (weeks to months) observations of the FBC overflow transport^{5,16,24,25}, and open circles show direct, near-synoptic transport estimates^{26–28}. Error bars show published error estimates for the respective observations when available. The observed FBC overflow series since 1995 are defined solely from the velocity field⁵. For the model series, additional temperature and salinity constraints have been applied⁶. These definitions are internally consistent and comparable to procedures used to obtain overflow transport estimates before 1995.

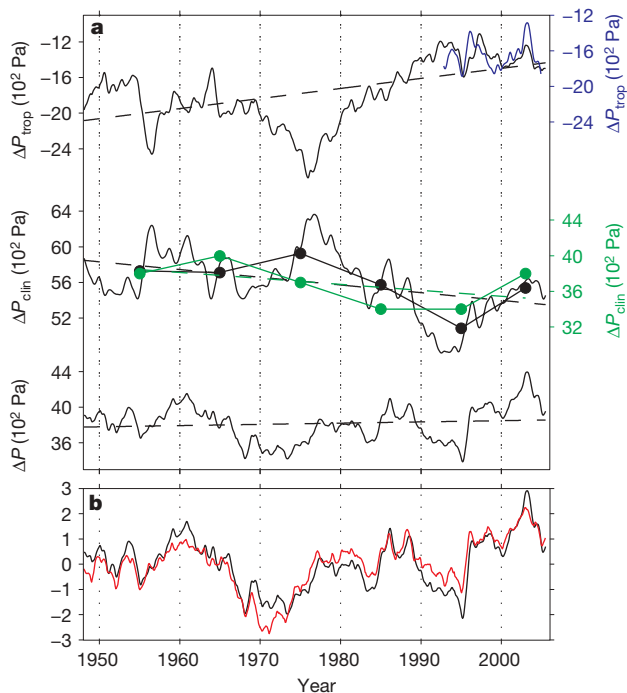


Figure 3 | Pressure forcing of the FBC overflow. **a**, Modelled (black) barotropic (ΔP_{trop}), baroclinic (ΔP_{clin}) and total (ΔP) pressure differences between both ends of the channel at the depth of the overflow core (750 m), evaluated from two remote positions in the Norwegian Sea and the Iceland basin (north minus south; for positions see Fig. 4). For ΔP_{clin} , decadal averages are included (circles) and compared with observed ΔP_{clin} (green) on the basis of hydrographic profiles extracted from the quality-controlled International Council for the Exploration of the Seas (ICES) database²⁹ near the two end points; note the different scales. For ΔP_{trop} , the modelled variability is compared with the observed gradient derived from altimetry (blue) for the period 1992–2005. Dashed lines represent linear regression fits to the model time series (black) and to the observed ΔP_{clin} (green). **b**, The direct pressure forcing of the modelled overflow transport is illustrated by comparing the evolution of the normalized pressure difference (black) and computed overflow transport (red). The correlation coefficient between pressure and flow is 0.90. The annual cycle is removed from the monthly model and altimetry data presented, and the time series have subsequently been low-pass filtered with a forward–reverse filter with a cutoff period of 12 months.

satellite altimetry since 1992 match the temporal evolution of the barotropic forcing simulated by the model fairly well (Fig. 3a) but the period is too short for a trend analysis. Hydrographic observations span the whole period, but they are sparse and inhomogeneous in time and space and do not permit the resolution of interannual variability. However, comparison between the model-derived and observational baroclinic pressure gradients does yield a similar level of inter-decadal variability and nearly identical, negative trends (Fig. 3a). This confirms that the model does not underestimate the decline in the baroclinic forcing of the overflow during the past five decades⁷. The comparison reveals an offset of about 20×10^2 Pa between model and observations (Fig. 3a). This discrepancy is intrinsic to the limited grid resolution of the model, which apparently overestimates the baroclinic (and hence total) cross-ridge pressure difference needed to drive a realistic eastern overflow. As long as this offset is not too large, it will not affect the shorter-term and longer-term variability of the transports, as indeed is suggested by the good correspondence between observations and the model (Fig. 2).

The compensation between barotropic and baroclinic pressure gradients has consequences for the future monitoring of the overflows. Monitoring of the hydrographic structure and sea-surface height alone²² is faced with the problem of disentangling the relatively small residual signal of interest as a difference of two larger, partly compensating, signals. At present, there is therefore no alternative to monitoring by direct current measurements.

In this paper we argue that the high correlation between observed and computed FBC overflow transports provides strong evidence that the model output is realistic. Strictly, this has only been proven for the FBC overflow in the period 1995–2005, but model validity for the total overflow and for the whole period 1948–2005 are supported by the available observations: overflow measurements in the Denmark Strait²⁰, historic FBC overflow estimates (Fig. 2b), satellite altimetry (Fig. 3a) and hydrographic observations (Fig. 3a).

The combined evidence from observations and model results indicates that neither the FBC overflow nor the total overflow transports had any consistent trends from 1948 to 2005. This is in conflict with the claim⁸ that the overflow contribution to the AMOC at 25° N weakened by 50% during this period. In the present climate, the overflows supply about one-third to the volume transport of the deep branch of the AMOC²³. Therefore any variations in the AMOC cannot be related to overflow variability but instead have to be produced by processes south of the GSR such as entrainment and Labrador Sea convection, each of which contribute about one-third to the AMOC.

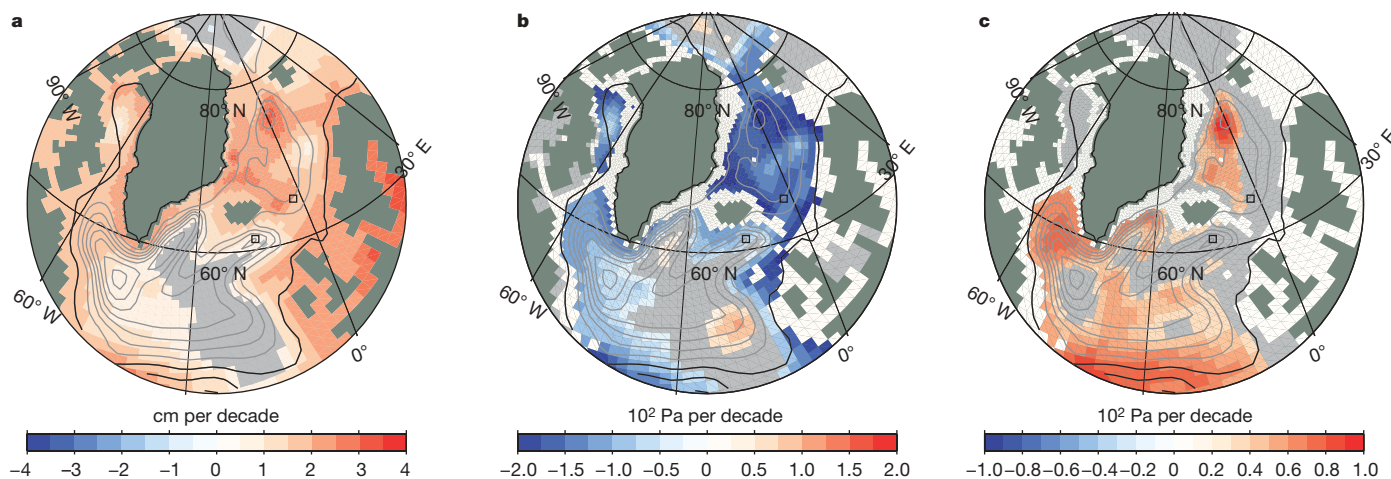


Figure 4 | Modelled long-term changes in the North Atlantic. Decadal tendencies calculated for the full period 1948–2005 are shown for sea-level (a), baroclinic (b) and total (c) pressure at a level representing the core of the FBC deep overflow (750 m). Regions where the trend is not significant are

shown in grey. The time-mean barotropic stream-function is depicted with cyclonic circulation indicated by grey lines. Transport between contours is 4 Sv. The squares mark the grid points between which pressure differences (Fig. 3) were calculated.

METHODS SUMMARY

We exploit an ensemble global ocean hindcast simulation⁶ with 26 members, using a coupled ocean–sea-ice model, forced by reanalysis data. The model configuration has coarse grid spacing, although enhanced horizontal resolution is achieved in the Nordic seas. The model grid does not resolve the various shallow overflows east of Iceland but has one channel that carries the total eastern overflow. The experiment is designed⁶ to isolate the forced ocean climate history by construction of the ensemble mean, thereby reducing the uncertainties arising from the initial state and internal model variability. The ensemble spread decreases over time⁶ (Fig. 2b), and short-term variability is largely unaffected by averaging (Supplementary Fig. 2). The resulting mean time series fits the observations extremely well (Fig. 2a), better than any individual member (Supplementary Fig. 1). We test the significance of our correlations between computed and observed FBC overflow and find the probability of obtaining a correlation coefficient of 0.72 for monthly, de-seasoned variability by chance to be less than 10^{-7} and the annual mean correlation of 0.92 to be less than 10^{-4} .

Compensation between barotropic and baroclinic changes (Fig. 3) is explained conceptually by using the linear relation between variations in simulated overflow transport and pressure difference between the relatively quiescent basin downstream of the channel and the Norwegian basin, upstream of the channel. An increase in sea level here increases the difference in barotropic pressure, and the associated increase in overflow transport implies an increased removal of overflow water from the basin. This causes the isopycnal surfaces to deepen, reducing the baroclinic pressure difference. If the Norwegian basin is approximated with a two-layer system, the timescale associated with this compensating effect is about three years.

Full Methods and any associated references are available in the online version of the paper at www.nature.com/nature.

Received 18 January; accepted 31 July 2008.

- Saunders, P. M. in *Ocean Circulation and Climate: Observing and Modelling the Global Ocean* (eds Siedler, G., Church, J. & Gould, J.) 401–417 (Academic, 2001).
- Dickson, R. R. & Brown, J. The production of North Atlantic Deep Water: Sources, rates, and pathways. *J. Geophys. Res.* **99**, 12319–12342 (1994).
- Gregory, J. M. *et al.* A model intercomparison of changes in the Atlantic thermohaline circulation in response to increasing atmospheric CO₂ concentrations. *Geophys. Res. Lett.* **32**, L12703, doi:10.1029/2005GL023209 (2005).
- Meehl, G. A. *et al.* in *Climate Change 2007: The Physical Science Basis. Contribution of Working Group I to the Fourth Assessment Report of the Intergovernmental Panel on Climate Change* (eds Solomon, S. *et al.*) 747–846 (Cambridge Univ. Press, 2007).
- Hansen, B. & Østerhus, S. Faroe Bank Channel overflow 1995–2005. *Prog. Oceanogr.* **75**, 817–856 (2007).
- Olsen, S. M. & Schmith, T. North Atlantic–Arctic Mediterranean exchanges in an ensemble hindcast experiment. *J. Geophys. Res.* **112**, C04010, doi:10.1029/2006JC003838 (2007).
- Hansen, B., Turrell, W. R. & Østerhus, S. Decreasing overflow from the Nordic seas into the Atlantic Ocean through the Faroe Bank channel since 1950. *Nature* **441**, 927–930 (2001).
- Bryden, H. L., Longworth, H. R. & Cunningham, S. A. Slowing of the Atlantic meridional overturning circulation at 25° N. *Nature* **438**, 655–657 (2005).
- Sherwin, T. J., Griffiths, C. R., Inall, M. E. & Turrell, W. R. Quantifying the overflow across the Wyville Thomson Ridge into the Rockall Trough. *Deep-Sea Res.* **55**, 396–404 (2008).
- Hermann, F. The T-S diagram analysis of the water masses over the Iceland–Faroe Ridge and in the Faroe Bank Channel (Overflow '60). *Rapp. P.-V. Réun. Cons. Int. Explor. Mer* **157**, 139–149 (1967).
- Meincke, J. On the distribution of low salinity intermediate waters around the Faroe. *Dt. Hydrogr. Z.* **31**, 50–64 (1978).
- Perkins, H., Hopkins, T. S., Malmberg, S.-A., Poulain, P.-M. & Warn-Varnas, A. Oceanographic conditions east of Iceland. *J. Geophys. Res.* **103**, 21531–21542 (1998).
- Marsland, S. J., Haak, H., Jungclaus, J. H., Latif, M. & Röske, F. The Max-Planck Institute global ocean/sea ice model with orthogonal curvilinear coordinates. *Ocean Model.* **5**, 91–127 (2003).
- Østerhus, S., Turrell, W. R., Jónsson, S. & Hansen, B. Measured volume, heat, and salt fluxes from the Atlantic to the Arctic Mediterranean. *Geophys. Res. Lett.* **32**, L07603, doi:10.1029/2004GL022188 (2005).
- Cunningham, S. A. *et al.* Temporal variability of the Atlantic meridional overturning circulation at 26.5°N. *Science* **317**, 935–937 (2007).
- Crease, J. The flow of Norwegian Sea Water through the Faroe Bank Channel. *Deep-Sea Res.* **12**, 143–150 (1965).
- Whitehead, J. A. Topographic control of oceanic flows in deep passages and straits. *Rev. Geophys.* **36**, 423–440 (1998).
- Girton, J. B., Pratt, L. J., Sutherland, D. A. & Price, J. F. Is the Faroe Bank Channel overflow hydraulically controlled? *J. Phys. Oceanogr.* **36**, 2340–2349 (2006).
- Käse, R. H. A Riccati model for Denmark Strait overflow variability. *Geophys. Res. Lett.* **33**, L21509, doi:10.1029/2006GL026915 (2006).
- Dickson, B. *et al.* in *Arctic–Subarctic Ocean Fluxes: Defining the Role of the Northern Seas in Climate* (eds Dickson, R. R., Meincke, J. & Rhines, P.) 443–474 (Springer, 2008).
- Jakobsen, P. K., Ribersgaard, M. H., Quadfasel, D., Schmith, T. & Hughes, C. W. The near-surface circulation in the northern North Atlantic as inferred from drifter data: variability from the meso-scale to interannual. *J. Geophys. Res.* **108**, 3251, doi:10.1029/2002JC001554 (2003).
- Köhl, A., Käse, R. & Stammer, D. Causes of changes in the Denmark Strait Overflow. *J. Phys. Oceanogr.* **37**, 1678–1696 (2007).
- Hansen, B., Østerhus, S., Quadfasel, D. & Turrell, W. Already the day after tomorrow? *Science* **305**, 953–954 (2004).
- Saunders, P. M. Cold outflow from the Faroe Bank Channel. *J. Phys. Oceanogr.* **20**, 29–43 (1990).
- Dooley, H. D. & Meincke, J. Circulation and water masses in the Faroe Channels during Overflow '73. *Dt. Hydrogr. Z.* **34**, 41–54 (1981).
- Sætre, R. *Report on the Norwegian investigations in the Faeroe Channel 1964–65* (NATO Subcommittee on Oceanographic Research, Tech. Rep. No. 38, 1967).
- Borenäs, K. A. & Lundberg, P. A. On the deep-water flow through the Faroe Bank Channel. *J. Geophys. Res.* **93**, 1281–1292 (1988).
- Saunders, P. M. Combining hydrographic and shipborne ADCP measurements. *Deep-Sea Res.* **39**, 1412–1427 (1992).
- International Council for the Exploration of the Seas. ICES Oceanogr. Database Services (<http://www.ices.dk/ocean/>) (2008).

Supplementary Information is linked to the online version of the paper at www.nature.com/nature.

Acknowledgements This work was partly supported by the European Commission as part of the MOEN (Meridional Overturning Exchange with the Nordic Seas) project, the Danish Environmental Ministry through the Danish Cooperation for Environment in the Arctic (DANCEA) programme, the Nordic Council in the project Arctic–Atlantic Exchanges (ARATEX), the German Federal Ministry of Education and Research (BMBF) in the North Atlantic Project, and the Research Council of Norway in the projects BIAC (Bipolar Atlantic Thermohaline Circulation) and POCAHONTAS (Polar Climate and Heat Transport). The altimeter products used were produced by Ssalto/DUacs and distributed by Aviso with support from CNES (<http://aviso.oceanobs.com>).

Author Contributions All authors contributed equally to this work.

Author Information Reprints and permissions information is available at www.nature.com/reprints. Correspondence and requests for materials should be addressed to S.M.O. (smo@dmu.dk).

METHODS

Model and ensemble approach. We exploit an ensemble global ocean hindcast simulation⁶ with 26 members, using a coupled ocean–sea-ice model, the Max Planck Institute Ocean Model¹³, forced by NCEP reanalysis data³⁰. The particular model configuration has on average a coarse grid spacing, although enhanced horizontal resolution is achieved in the Nordic seas by displacing the model North Pole. The model grid does not resolve the various shallow overflows east of Iceland; it has one channel that carries the total eastern overflow. No restoring of ocean properties is used, but to account for missing run-off and to correct for model deficits a static correction of the evaporation–precipitation field is applied⁶. The numerical experiment has been described in detail elsewhere⁶.

From an ensemble simulation, there are two basic approaches for achieving a good estimate of state variables and derived quantities. Ensemble members with optimal initial conditions may well represent real ocean characteristics and one might seek to identify these members. This is not necessarily the case for a forced experiment using a decoupled model system and was not the strategy pursued here for the ocean hindcast. Furthermore, model noise is introduced by the discrete time-stepping in combination with several highly nonlinear parameterizations of unresolved physical processes in the discretized numerical model of the mathematical governing (primitive) equations, and no single simulation can be expected to reflect directly observed changes. Hence, by constructing the ensemble mean, the experimental design⁶ allows us to isolate the forced ocean variability and strongly reduces the uncertainty and noise arising from the initial state and internal model variability³¹. Although noise is expected, it is not certain to what extent the noise interacts with the forced variability, and ensemble mean data should be used with caution. A detailed analysis of the characteristics of the internal variability has not been pursued because we find that the ensemble spread of key variables shows a clear decrease in time⁶ (Fig. 2b) and that the level of short-term variability is largely unaffected (Supplementary Fig. 2). In addition, convergence of the ensemble mean statistics for increasing ensemble size initially follows the scaling of an infinite synthetic ensemble with random noise added to the ensemble mean (Supplementary Fig. 2), which indicates negligible interaction between internal and forced variability. In corroboration, the ensemble mean time series fits the observations extremely well (Fig. 2a), better than any individual member (Supplementary Fig. 1). The correspondence is not really surprising, confirming that the FBC overflow is strongly forced, in the model and in nature. Model internal variability present in the individual members' estimates is strongly reduced in the ensemble mean (Supplementary Fig. 2). Internal model variability is 0.21 Sv, estimated as the mean standard deviation between ensemble members and the mean (σ_A ; Supplementary Fig. 2), whereas the model-generated variability remaining after averaging is only about 0.04 Sv.

Statistical significance and implications. Standard formulae are available for testing the significance of our correlations between computed and observed FBC overflow. When comparing the two time series, one has to account for seasonality and autocorrelation, which reduces the degrees of freedom. For the overlapping period 1995–2005, we identify near-identical seasonality in the model and observational data, with total variations of 0.57 and 0.58 Sv, respectively, both with a well-defined maximum in August. When constructing two new time

series by removing the seasonality from both observation and model data, the correlation is 0.72. Here the effective number of degrees of freedom³² is reduced to 39 in comparison with the full sample size of 127 monthly values, corresponding to a decorrelation timescale³² of 3.2 months. Using standard formulae, we estimate that the probability of getting this correlation of 0.72 for the monthly variability by chance is less than 10^{-7} . Similarly, autocorrelation is insignificant in the annual mean series, which implies that the probability of getting a correlation coefficient as high as 0.92 is less than 10^{-4} . We can therefore state beyond any reasonable doubt that the correlations between model and observations do not occur by chance, implying that the model does indeed represent the dynamic scales responsible for variations in the FBC overflow on monthly, seasonal and interannual scales. Furthermore, modelled variability is not significantly affected by the offset dictated by the climatic mean of unresolved contributions to the total eastern overflow.

A conceptual framework to explain the barotropic/baroclinic pressure compensation. Variations in the simulated FBC overflow transport Δq and pressure difference $\Delta P = \Delta P_{\text{trop}} + \Delta P_{\text{clin}}$ between the relatively quiescent basin downstream of the channel and the Norwegian basin, upstream of the channel, are close to being linearly related at the depth of the overflow (Fig. 3b): $\Delta q = k\Delta P$, where k is about 10^{-3} Sv Pa⁻¹. If sea level in this basin rises by Δh , the pressure difference increases by $\rho g\Delta h$. The associated increase in overflow transport enhances the removal of deep water from the basin, which causes the isopycnal surfaces to deepen, thereby reducing the baroclinic (ΔP_{clin}) component of the pressure difference. To quantify this compensating effect, we approximate the Norwegian basin by a two-layer system with density difference $\Delta\rho$. In this framework, average isopycnal deepening during a period T is equivalent to a deepening (ΔD) of the interface. If A is the area of the interface between the overflow and upper layer, the decrease in the baroclinic pressure difference follows from continuity:

$$\Delta P_{\text{clin}} = -g\Delta\rho\Delta D = \frac{-g\Delta\rho kT}{A}\Delta P_{\text{trop}} \quad (1)$$

To compensate for the barotropic pressure difference change, the fraction on the right-hand side of (1) should equal unity. This gives a rough estimate of the time T needed for the baroclinic field to respond to an induced change in sea-level difference across the ridge and for the overflow to return to its original value.

Using the area defined by the 500-m isobath (5.8×10^{11} m²) of the Norwegian basin for the interface area and a typical value of 0.5 kg m^{-3} for $\Delta\rho$, T is about 3 years. This conceptual framework therefore explains the compensation between barotropic and baroclinic contributions to the cross-ridge pressure difference evident in Fig. 3a on these timescales. On longer timescales, the overflow would then be determined by the import of dense water to the Norwegian basin.

30. Kistler, R. E. et al. The NCEP–NCAR 50-year reanalysis: Monthly means CD-ROM and documentation. *Bull. Am. Meteorol. Soc.* **82**, 247–268 (2001).
31. Vellinga, M., Dickson, B. & Curry, R. in *Arctic–Subarctic Ocean Fluxes: Defining the Role of the Northern Seas in Climate* (eds Dickson, R. R., Meincke, J. & Rhines, P.) 289–313 (Springer, 2008).
32. von Storch, H. & Zwiers, F. W. *Statistical Analysis in Climate Research* (Cambridge Univ. Press, 1999).